Coupling Exothermic and Endothermic Reactions in Plug-Flow Reactor−Separation−Recycle Systems

Pietro Altimari[†] **and Costin Sorin Bildea***[,†,‡]

Delft University of Technology, Julianalaan 136, 2628BL, Delft, The Netherlands, and University "Politehnica" of Bucharest, 1-7 Polizu, 011061 Bucharest, Romania

The nonlinear behavior of plug-flow reactor−separation−recycle systems, where the endothermic first-order reaction A → R + Q and the exothermic second-order reaction B + Q → P simultaneously take place, is investigated. As the physical properties of the species involved vary, possible flowsheets are identified and feasible control strategies are suggested. Bifurcation analysis of the reactor−separation−recycle system is performed by choosing set-point variables as bifurcation parameters. Steady state multiplicity is invariably detected leading to complex behavior. Implications on plantwide control are thoroughly discussed and guidelines are provided which enable to select values of set-point variables in a way that guarantees safe operation.

1. Introduction

The increasing demand of highly efficient and size-contained process facilities had lead over the past decades several researchers to review the traditional formulation of many chemical processes by investigating the possibility of direct coupling of endothermic and exothermic reactions. This guarantees, in general, improved thermal efficiency and, for reversible reactions, can lead to increased equilibrium conversion and reaction rate due to equilibrium displacement.[1] As a result, energy savings and reduced reactor size can be achieved. Some examples demonstrating the effectiveness of this idea are in situ hydrogen combustion in oxidative dehydrogenation;[2–4] coupling propane combustion and endothermic thermal cracking of propane to ethylene and propylene;[5] coupling methane steam reforming with catalytic oxidation of methane in partial oxidation reactors;[6–8] coupling ethylbenzene dehydrogenation with water−gas shift, CO_2 methanation, and nitrobenzene hydrogenation.[9]

However, while enhancing reactor performance, coupling endothermic and exothermic reactions in a single unit may lead to higher complexity of the external plant, making necessary additional separation units and recycles. In practice, energy savings and reduced reactor investments must outweigh the cost of required additional units. Furthermore, operational and control difficulties arising from a more complex behavior should be taken into account to assess the feasibility of this operation mode. To this regard, it is important to remark that several previous studies showed the recycle of unconverted reactants to be the cause of undesired nonlinear phenomena in plantwide systems.

In this framework, Pushpavanam and Kienle[10] analyzed the dynamic behavior of a continuously stirred tank reactor (CSTR)−separation−recycle system where a first-order exothermic reaction takes place. They presented 25 bifurcation diagrams exhibiting a maximum of two coexisting steady states, two isolated steady state solution branches, and Hopf bifurcations giving rise to periodic solution regimes. Kiss et al.[11,12] showed that, as result of material recycles, nonlinear phenomena can arise in CSTR−separation−recycle and plug-flow reactor (PFR)−separation−recycle systems where complex reactions take place. The importance of these results for design and control was thoroughly discussed by Bildea and Dimian.[13] They investigated the nonlinear behavior of several systems involving first- and second-order exothermic reactions, providing detailed explanations of some control difficulties addressed by previous plantwide control studies.[14]

Besides the singularity theory, we also mention recent approaches to modeling and control of plantwide systems, namely based on irreversible thermodynamics[15,16] and on multiscale analysis.[17,18]

However, despite the increasing interest toward the development of intensified process systems by direct coupling of exothermic and endothermic reactions, research in this field has been mainly focused on the efficient design and analysis of stand-alone reactor units, while no studies concerning the implementation of this operation mode in plantwide systems have been reported.

In this work, we investigate the steady state behavior of reactor−separation−recycle systems where an endothermic first-order reaction and an exothermic second-order reaction take place:

$$\mathrm{A} \rightarrow \mathrm{R} + \mathrm{Q} \qquad \Delta H_1 > 0$$

$$\mathrm{B} + \mathrm{Q} \rightarrow \mathrm{P} \qquad \Delta H_2 < 0$$

This reaction scheme is representative of a large class of chemical processes of practical relevance, where the heat required to perform a desired endothermic reaction is provided by conversion of a byproduct (Q) in a second exothermic reaction. In particular, the stoichiometry of important industrial reactions such as dehydrogenation or cracking is similar to the first reaction of the scheme considered in this study, while the kinetics is first-order. A second-order exothermic reaction is selected to describe the combination of the reactant B with the byproduct Q because this is a practical way to provide the heat necessary for the first reaction, and also to shift the chemical equilibrium due to consumption of the species Q.

The paper is structured as follows. In section 2, flowsheets of the reactor−separation−recycle system which are possible, depending on the physical properties of the species involved, are analyzed and feasible control strategies are suggested. In

* To whom correspondence should be addressed. Present address: University "Politehnica" of Bucharest, Department of Chemical Engineering, 1-7 Polizu Street, 011061 Bucharest, Romania. Tel.: +40 21 4023903. Fax: +40 21 3185900. E-mail: s_bildea@upb.ro.

[†] Delft University of Technology.

[‡] University Politehnica of Bucharest.

10.1021/ie071367g CCC: $40.75
Published on Web 08/02/2008

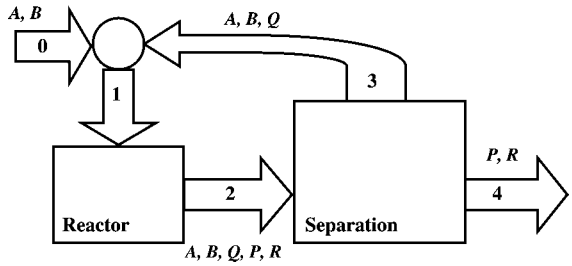

Figure 1. General structure of reactor−separation−recycle systems.

section 3, model equations are presented in dimensionless form. The main results are presented in section 4, where the steady state behavior of the reactor−separation−recycle system is described and operational difficulties are addressed. Final remarks end the paper.

2. Conceptual Design and Plantwide Control

We consider the endothermic first-order reaction A → R + Q and the exothermic second-order reaction B +Q → P taking place in a plug-flow reactor. The reactants A and B are fed to the plant while the amount of the species Q required to perform the exothermic reaction is provided by the endothermic reaction.

Disregarding the details of the separation section, the system can be described by the block diagram displayed in Figure 1. Throughout the paper, $f_{K,I}$ (K = A, B, Q and I = 0, 1, 2, 3, 4) will denote the dimensionless molar flow rate of the species K in the stream I. The separation section is represented by a black box and a unique stream is employed for the recycle of reactants A, B, Q. We assume that unconverted reactants A, B, and Q are recovered and recycled to the reactor, while products P and R are removed from the plant. This assumption is realistic because in practice P and R are usually withdrawn as high-purity product streams, containing only small amounts of reactants A, B, and Q. On the other hand, the size of recycles and therefore the cost of recycling are minimized when the products P and R are excluded from the recycle streams.

In the fulfillment of the previous requirements, we assume that separation units are properly designed and controlled to remove state multiplicity of the stand-alone separation section and to keep the desired separation specifications as plant operating conditions are quasi-statically varied. The first assumption is in line with the hierarchical character of plantwide control which always employs local control to change the complex behavior of open-loop units into an ideally linear behavior of the closed loop units.[20] Furthermore, standard process flexibility requirements make the latter assumption holding, in practice, within a large region surrounding the plant nominal operating point. To this regard, it should be observed that, in industrial practice, separation units are designed to face large variations of internal plant flow rates resulting, for example, from changes of plant productivity.

It is worth noting that the assumption of a priori fixed separation performances only defines the amount of reaction products in the recycle streams and, hence, does not rule out the possibility of interaction between separation and reactor units which is the main source of complexity in reactor−separation−recycle systems. As plant operating conditions are varied, changes in the flow rates of the recycle streams and their compositions will be observed, even if the concentrations of the reaction products in the recycle streams are kept constant. When a thorough selection of the plant control structure and/or of design and control parameters is not performed, these changes will be shown to be responsible of undesired nonlinear phenomena as, for example, steady state multiplicity and unfeasible operating ranges.

In this framework, it is also important to observe that deviations of the compositions of reaction products in the recycle streams from their stationary values can transitorily arise due to the dynamics of the separation units. If effective control strategies are not implemented to reduce the effects of these transients on reactor dynamics, autonomous periodic, quasi-periodic, and chaotic oscillations can occur, leading, for example, to plant shutdown, runaway reactions, and catalyst deactivation. However, formulating solutions to reduce the risk of these undesired dynamics goes beyond the scope of this work. This contribution is rather aimed to investigate the effects of the direct coupling of exothermic and endothermic reactions on the asymptotic behavior of reactor−separation−recycle systems. With this objective, the existence of unfeasible operating regions and the occurrence of state multiplicity are thoroughly investigated providing valuable information for plant operation and control. In order to understand the relevance of this analysis, it is sufficient to observe that when the plant is operated at a stationary point close to a saddle node bifurcation, a slight disturbance of the operating conditions can lead to a sudden variation of the state variables. In this scenario, a significantly large deviation from the nominal operating point might give rise, for example, to saturation of the feedback controllers, making the actuators unable to provide implementation of the control law. Under these conditions, the plant behaves as uncontrolled and additional undesired nonlinear phenomena can occur.

Following the plant flowsheet described in Figure 1, mole balance equations governing the steady state behavior of the reactor−separation−recycle system can be written as follows:

$$f_{A,1} - f_{A,0} - \Phi_A = 0 \tag{1}$$

$$f_{B,1} - f_{B,0} - \Phi_B = 0 \tag{2}$$

$$f_{Q,1} - \Phi_Q = 0 \tag{3}$$

Φ_A, Φ_B, and Φ_Q are functions describing the dependence of recycle flow rates $f_{A,3}$, $f_{B,3}$, and $f_{Q,3}$ on reactor-inlet flow rates $f_{A,1}$, $f_{B,1}$, and $f_{Q,1}$, reactor parameters, and separation performance. Five unknown lumped variables are to be determined from three equations. Hence, two consistent specifications must be provided to solve the balance equations.

In practice, these specifications could be achieved by flow or concentration control loops. However, since concentration measurements are expensive and unreliable, controlling flow rates is in general the preferred option.[19] For this reason, we define as admissible the control strategies which can be applied without using concentration measurements.

It is important to observe that, although the structure of the separation section does not affect the number of specifications which must be provided to solve mole balance equations, it might restrict the control strategies which can be applied. For example, if the separation section delivers a single recycle stream containing the species A and B, fixing the recycled amount of A (or B) is not feasible because it requires a concentration measurement. Therefore, the set of admissible control strategies which can be applied is determined by the number of recycle streams and their components.

The structure of the separation section is determined by the physical properties of the species involved. For example, assuming that separation is done by distillation, Figure 2 displays detailed flowsheets corresponding to two different rankings of relative volatilities.

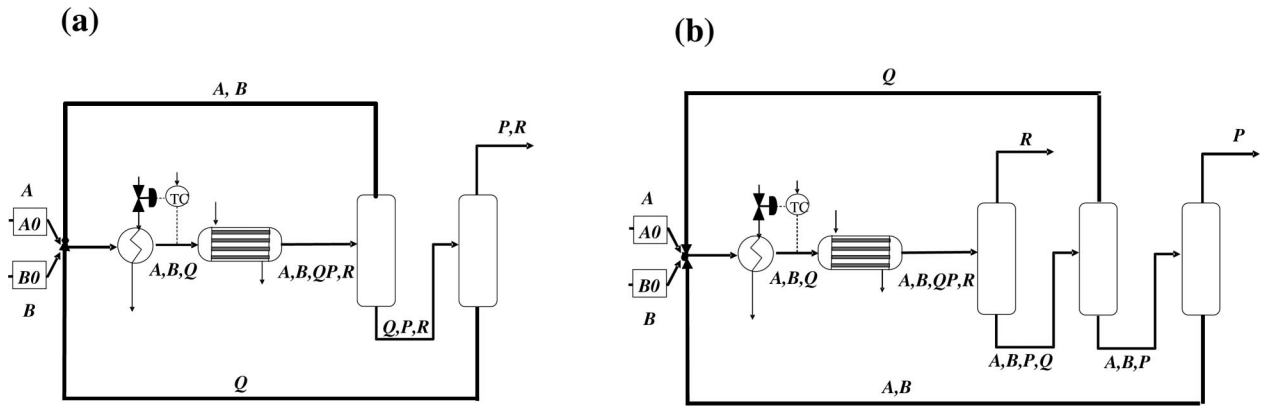

Figure 2. Flowsheets of the PFR−separation−recycle system corresponding to different rankings of relative volatilities of the species involved: (a) $\alpha_Q < \alpha_R < \alpha_P < \alpha_A < \alpha_B$; (b) $\alpha_A < \alpha_B < \alpha_P < \alpha_Q < \alpha_R$.

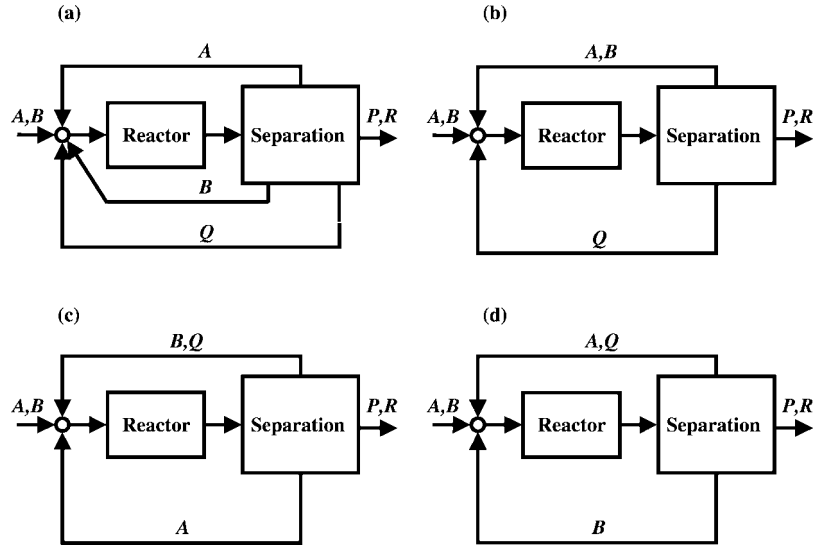

Figure 3. Classification of the flowsheets of the PFR−separation−recycle system which are possible as the ranking of relative volatilities of the species involved varies. (a) The reactants A, B, and Q are recycled by three distinct streams; (b) The reactants A and B are recycled by a unique stream; (c) The reactants B and Q are recycled by a unique stream; (d) The reactants A and Q are recycled by a unique stream.

When the ranking of relative volatilities is $\alpha_Q < \alpha_R < \alpha_P < \alpha_A < \alpha_B$ (Figure 2a), separation can be performed by two units, while three units are required when the relative volatilities are ordered as $\alpha_A < \alpha_B < \alpha_P < \alpha_Q < \alpha_R$ (Figure 2b). However, the two flowsheets exhibit identical recycle streams.

The previous example shows that reactor−separation−recycle systems with different structures of the separation section could present the same recycle streams. In this case, identical admissible control strategies apply to them. On the basis of this example, it is useful, while identifying admissible control strategies, to structure the set of possible flowsheets according to the classes described in Figure 3.

Here, the recycle streams and their components are specified, but details concerning the structure of the separation section are not reported. Each class described in Figure 3 groups flowsheets exhibiting different structures of the separation section. Flowsheets belonging to a given class are equivalent in the sense that they present identical recycle streams, and hence, the same admissible control strategies apply to them. In this perspective, the analysis of the classes presented in Figures 3a−d is sufficient to determine all the admissible control strategies which can be implemented.

In order to identify admissible control strategies, the following remarks need to be preliminarily provided:

- We assume that separation is performed by distillation. Hence, recycles are distillate or bottom streams which are commonly employed as manipulated variables for condenser or reboiler level control, respectively. For this reason, we exclude from our analysis control strategies fixing recycle flow rates. Motivated by this and taking into account that no fresh Q is fed to the plant, fixing the reactor-inlet flow rate of Q is unfeasible even when Q is recycled by a separate stream (Figure 3a and b).

- According to reaction stoichiometry and the global mole balance, reactants A and B must be fed exactly in a one-to-one ratio. In practice, unavoidable control implementation errors make the strategy fixing both fresh feeds of the reactants A and B unfeasible.

- While formulating admissible control strategies, we will attempt to minimize the number of species mixed in the same vessel.

Controlling the inventory of reactants within the plant can be performed in two ways:[13] (a) by evaluating, directly or indirectly, the inventory of each reactant and controlling it by feedback using the corresponding fresh feed as manipulated variable and (b) by fixing the fresh feed rate and using the self-regulation property of the mass balance.[21] The latter assumes that the entire amount of reactant brought into the process is converted into products, which are subsequently separated and removed from the plant.

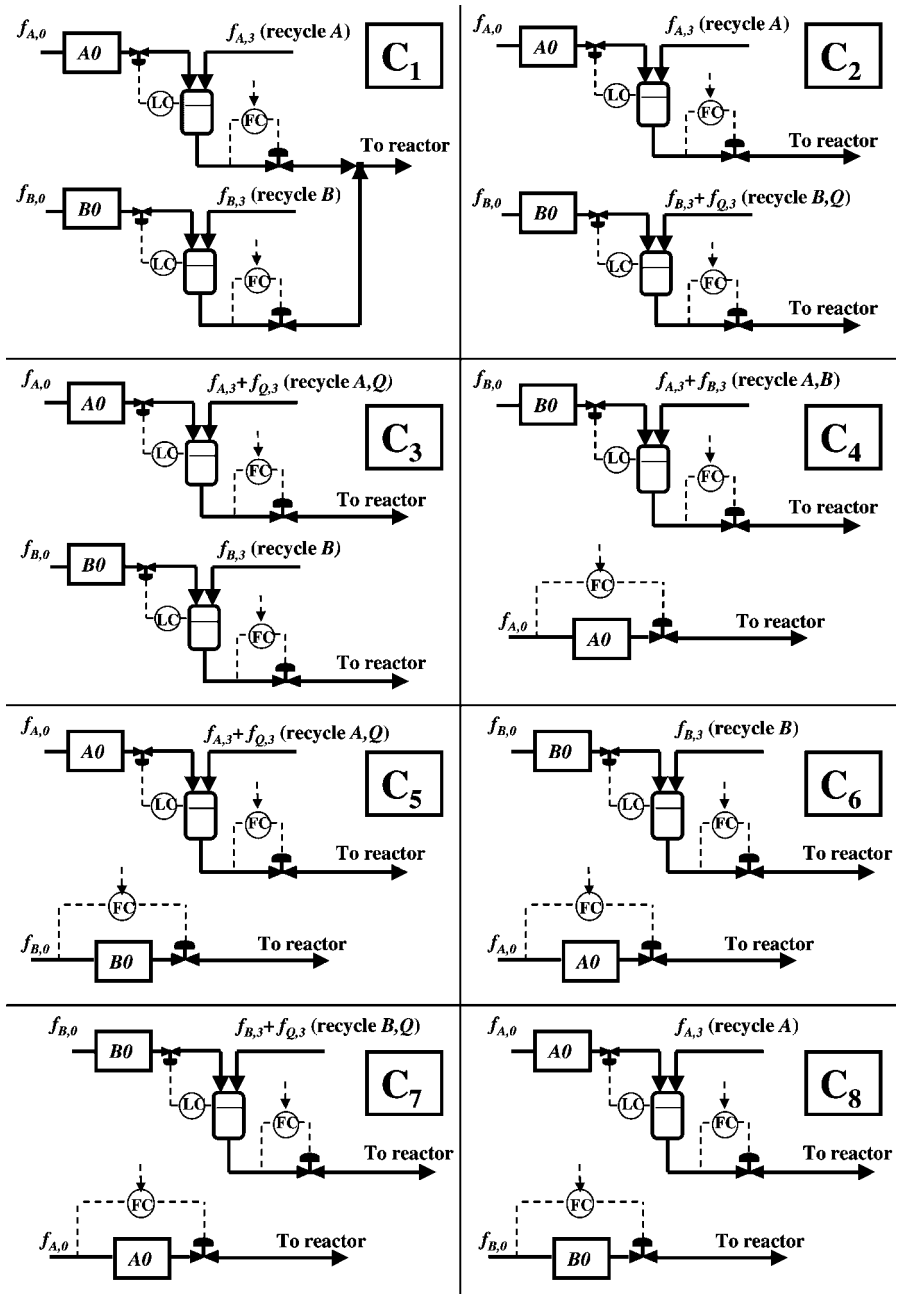

Figure 4. Control structures of the reactor−separation−recycle system.

Following the previous comments, we describe in Figure 4 eight admissible control strategies. Flow rate specifications provided by the proposed strategies and flowsheet classes to which they apply are presented in Table 1 distinguishing between strategies where the inventory of both reactants is controlled by feedback (C_1, C_2, C_3) and strategies exploiting the self-regulation property (C_4, C_5, C_6, C_7, C_8).

3. Mathematical Model

In this section, we present the mathematical model governing the steady state behavior of the reactor−separation−recycle system. The main assumptions behind the formulation of the model are listed as follows:

- According to the usual industrial practice, the reactor-inlet temperature is fixed by the local control of a heat exchanger placed upstream the reactor. It should be also observed that keeping the reactor inlet temperature under control is indispensable to remove energy feedback effects which have been extensively recognized to be source of undesired nonlinear phenomena during reactor operation.

- A plug-flow model is used to describe the steady state behavior of the reactor. This model, in its steady state version, is defined by an initial value problem and, hence, does not admit multiple coexisting solutions. With this choice, the detection of stationary bifurcations of the reactor−separation−recycle system must be mainly attributed to the interaction between mass recycles and direct reaction coupling.

- First-order kinetics for the endothermic chemical reaction A → R + Q ($r_A = k_1 w_A$), second-order kinetics for the exothermic chemical reaction B + Q → P ($r_B = k_2 w_B w_Q$), and Arrhenius dependence of the kinetic constants on temperature are assumed.

On the basis of the previous assumptions, mass and energy balance equations describing the steady state behavior of the reactor−separation−recycle system are written as follows:

Mass and energy balance equations along the chemical reactor:

$$\frac{df_A}{d\xi} = -Da \exp\left(\frac{\theta\gamma}{1+\theta}\right)\frac{f_A}{f} \quad (4)$$

$$\frac{df_B}{d\xi} = -DaK_{2,1} \exp\left(\frac{\theta\gamma G_{2,1}}{1+\theta}\right)\frac{f_Q f_B}{f^2} \quad (5)$$

$$\frac{d\theta}{d\xi} = \frac{Da}{f}\left[K_{2,1}H_{2,1}B \exp\left(\frac{\theta\gamma G_{2,1}}{1+\theta}\right)\frac{f_Q f_B}{f^2} - B \exp\left(\frac{\theta\gamma}{1+\theta}\right)\frac{f_A}{f} - \beta(\theta-\theta_c)\right] \quad (6)$$

$$f_Q = f_{Q,1} + (f_{A,1} - f_A) - (f_{B,1} - f_B);$$
$$f_R = (f_{A,1} - f_A);$$
$$f_P = (f_{B,1} - f_B) \quad (7)$$

$$f = f_A + f_B + f_Q + f_P + f_R \quad (8)$$

Boundary reactor conditions:

$$f_A(0) = f_{A,1};$$
$$f_B(0) = f_{B,1};$$
$$f_{A,2} = f_A(1);$$
$$f_{B,2} = f_B(1);$$
$$f_{Q,2} = f_Q(1) \quad (9)$$

Mole balance equations for the separation section:

$$f_{A,2} - f_{A,3} = 0 \quad (10)$$

$$f_{B,2} - f_{B,3} = 0 \quad (11)$$

$$f_{Q,2} - f_{Q,3} = 0 \quad (12)$$

Mole balance equations for the mixing point:

$$f_{A,0} + f_{A,3} - f_{A,1} = 0 \quad (13)$$

$$f_{B,0} + f_{B,3} - f_{B,1} = 0 \quad (14)$$

$$f_{Q,3} - f_{Q,1} = 0 \quad (15)$$

The variables appearing in the mathematical model are the dimensionless axial coordinate $\xi = z/L$, $0 < \xi < 1$, the dimensionless flow rates $f_A = F_A/F_0$, $f_B = F_B/F_0$, $f_Q = F_Q/F_0$ and temperature $\theta = (T - T_1)/T_1$ along the reactor, the dimensionless reactor-inlet flow rates $f_{A,1} = F_{A,1}/F_0$, $f_{B,1} = F_{B,1}/F_0$, $f_{Q,1} = F_{Q,1}/F_0$, and the dimensionless recycle flow rates $f_{A,3} = F_{A,3}/F_0$, $f_{B,3} = F_{B,3}/F_0$, $f_{Q,3} = F_{Q,3}/F_0$. The model parameters are the Damköhler number $Da = k_1(T_1)V/F_0$, the ratio between the kinetic constants $K_{2,1} = k_2(T_1)/k_1(T_1)$, the dimensionless adiabatic temperature rise $B = \Delta H_1/C_pT_0$, the ratio between the reactions enthalpies $H_{2,1} = -\Delta H_2/\Delta H_1$, the dimensionless heat transfer capacity $\beta = UL/k_1C_pA$, and the dimensionless cooling temperature $\theta_c = (T_c - T_1)/T_1$. It should be observed that the reactor inlet temperature, which is assumed to be kept constant, is here used as reference value for the definition of the dimensionless temperature.

Equations 4 and 5 are formulated based on the general flowsheet displayed in Figure 1 and, hence, invariably apply as the recycle structure is varied. After rearranging eqs 10–15, the mathematical model governing the steady state behavior of the reactor−separation−recycle system can be recast in the compact form presented in eqs 1–3. $(\Phi_A, \Phi_B, \Phi_Q) \equiv (f_{A,3}, f_{B,3}, f_{Q,3}) \equiv \Phi(f_{A,1}, f_{B,1}, f_{Q,1}, \theta_c, Da, B, K_{1,2}, H_{1,2}, \gamma, \beta)$ results from integration of the plug-flow model eqs 4–9 and solution of the separation model eqs 10–12 describing the dependence of recycle flow rates on reactor-inlet flow rates, reactor parameters, and separation performances. Equations 1–3 contain five lumped variables ($f_{A,0}$, $f_{B,0}$, $f_{A,1}$, $f_{B,1}$, $f_{Q,1}$). Therefore, two additional equations must be provided in order to solve mole balance equations.

Control strategies presented in section 2 describe different ways to write the required additional equations defining relationships between the unknown lumped variables appearing in eqs 1–3.

Table 1. Control Structures of the PFR−Separation−Recycle System

Reactants Inventory Controlled by Feedback		
control strategy	flow rates specifications	flowsheet classes
C_1	$f_{A,1} - m = 0$ $f_{B,1} - p = 0$	Figure 3**a**
C_2	$f_{A,1} - m = 0$ $f_{B,1} + f_{Q,1} - p = 0$	Figure 3**a and c**
C_3	$f_{B,1} - m = 0$ $f_{A,1} + f_{Q,1} - p = 0$	Figure 3**a and d**
Inventory of One Reactant Self-Regulating		
control strategy	flow rates specifications	flowsheet classes
C_4	$f_{A,0} - m = 0$ $f_{B,1} + f_{A,3} - p = 0$	Figure 3**a and b**
C_5	$f_{B,0} - m = 0$ $f_{A,1} + f_{Q,1} - p = 0$	Figure 3**a and d**
C_6	$f_{A,0} - m = 0$ $f_{B,1} - p = 0$	Figure 3**a and d**
C_7	$f_{A,0} - m = 0$ $f_{B,1} + f_{Q,1} - p = 0$	Figure 3**a and c**
C_8	$f_{B,0} - m = 0$ $f_{A,1} - p = 0$	Figure 3**a and c**

4. Influence of the Set-Point Variables *m* and *p*

In this section, we present results of the bifurcation analysis of the PFR−separation−recycle system as the set-points m and p of the flow control loops are varied. Motivating this study, we remark that, when reactor parameters are fixed, the steady state behavior of the system is governed by parameters m and p. Hence, guidelines to select m and p need to be provided. With this objective, we derive, based on bifurcation analysis, simple rules to fix m and p in a way that guarantees feasible operation. The discussion is structured by distinguishing between strategies based on feedback control of reactants inventory (C_1, C_2, C_3) and control strategies exploiting self-regulation (C_4, C_5, C_6, C_7, C_8).

In subsection 4.1, we present results concerning the steady state behavior of the reactor−separation−recycle system controlled by strategies C_1−C_3, while the bifurcation structure of the system controlled by strategies C_4−C_8 is described in subsection 4.2.

4.1. Control Strategies Based on Feedback Control of Reactants Inventory. Control Strategy C_1. The model to be solved in order to determine the steady state solution regimes of the PFR−separation−recycle system controlled by strategy C_1 is described by equations 1–3 and the following additional equations:

$$f_{A,1} - m = 0 \quad (16)$$

$$f_{B,1} - p = 0 \quad (17)$$

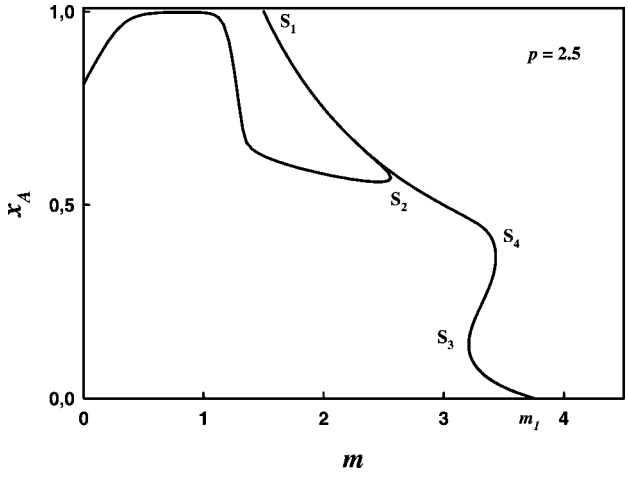

Figure 5. Steady state solution diagram of the PFR−separation−recycle system controlled by strategy C_1, with m as the bifurcation parameter. ($Da = 2.5$, $K_{2,1} = 2.5$, $B = 0.3$, $\beta = 0.5$, $\gamma = 12.5$, $G_{2,1} = 2.5$, $H_{2,1} = 4.5$, $\theta_c = 0$).

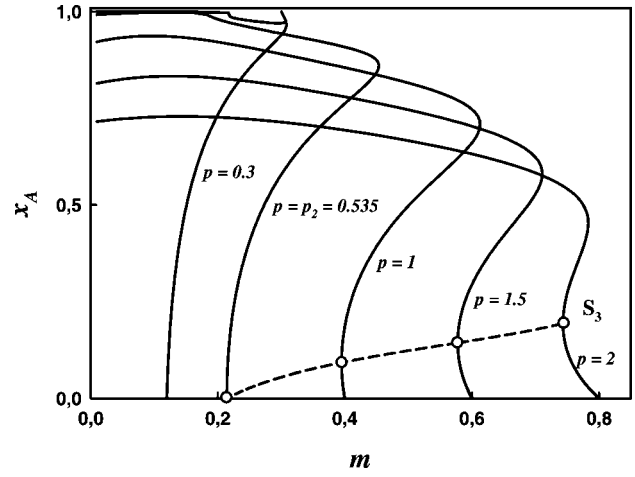

Figure 7. Steady state solution diagrams of the PFR−separation−recycle system controlled by strategy C_1, with m as a bifurcation parameter, computed by varying p at $K_{2,1} = 0.4$. ($Da = 2.5$, $B = 0.3$, $\beta = 0.5$, $\gamma = 12.5$, $G_{2,1} = 2.5$, $H_{2,1} = 4.5$, $\theta_c = 0$).

where m and p define the reactor-inlet flow rates of A and B, respectively. Typical steady state solution regimes are described in Figure 5 as m varies, at $p = 2.5$. The reactor conversion of A is employed as variable representative of the state of the system. Four saddle-node bifurcation points S_1, S_2, S_3, and S_4 are predicted.

A unique steady state is found at low m values. As m is increased, three coexisting steady states are detected between the points S_1 and S_2. In this range, two coexisting regimes exhibit very close conversion values resulting barely distinguishable in Figure 5. At larger m values, a unique steady state is detected in the range delimitated by the points S_2 and S_3. As m is further increased, three coexisting steady states arise between the points S_3 and S_4. After the saddle-node bifurcation point S_4, a unique steady state is detected at m values lower than m_1. Increasing m in this range, the reactor conversion becomes smaller and smaller and approaches zero in the limit $m \rightarrow m_1$. No feasible steady states are detected at larger m values.

The solution diagram displayed in Figure 5 proves that the reactor−separation−recycle system controlled by strategy C_1 exhibits a complex steady state behavior. To this regard, it is remarkable that C_1 is, in general, the recommended strategy when coping with reactor−separation−recycle systems.[13] The argument for this is that fixing the reactor-inlet flow rates of the reactants removes the effect of mass recycle. As a result, the system is expected to behave as a plug-flow reactor followed

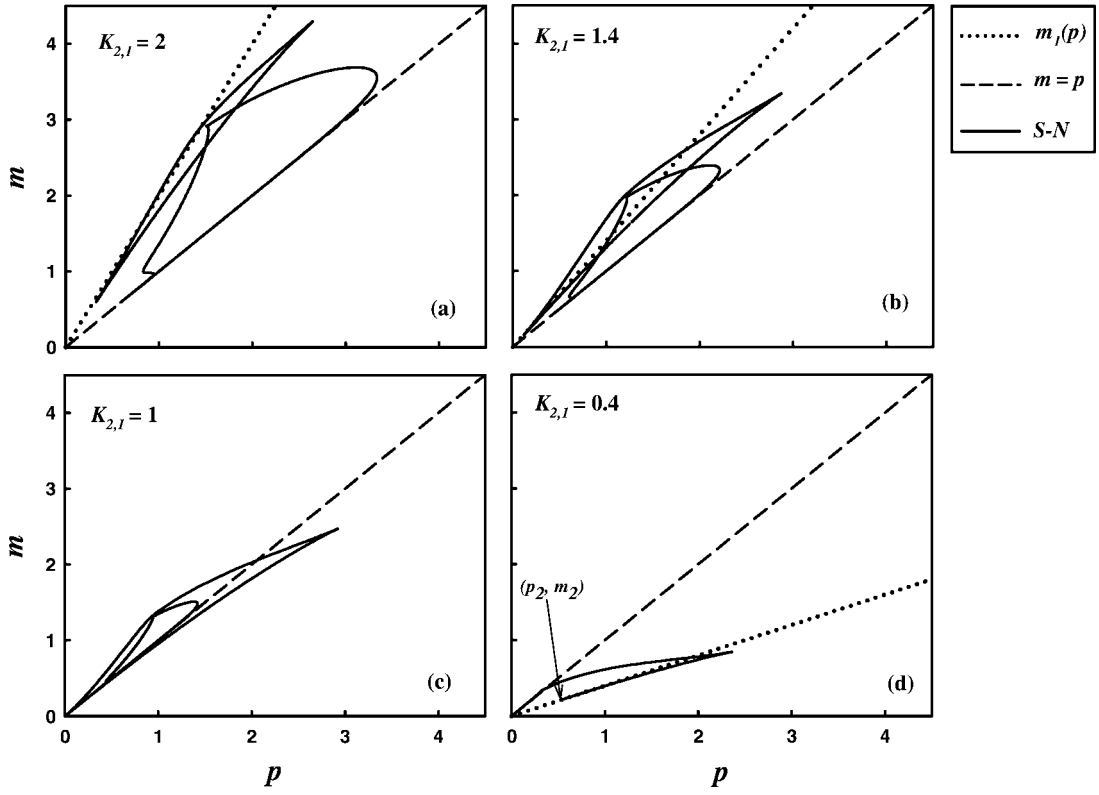

Figure 6. Projections of the saddle node bifurcation points of the PFR−separation−recycle system controlled by strategy C_1 on the $m-p$ plane as $K_{2,1}$ varies: (a) $K_{2,1} = 2$; (b) $K_{2,1} = 1.4$; (c) $K_{2,1} = 1$; (d) $K_{2,1} = 0.4$ ($Da = 2.5$, $B = 0.3$, $\beta = 0.5$, $\gamma = 12.5$, $G_{2,1} = 2.5$, $H_{2,1} = 4.5$, $\theta_c = 0$).

by a separation section, which exhibits a unique steady state. However, for the reaction scheme here considered, the effect of recycling the intermediate species Q is still present, leading to the observed complex behavior.

In Figure 5, feasible steady states are always observed at m values lower than m_1. Hence, m_1 can provide useful indications to select m values guaranteeing feasible operation. Analytic prediction of m_1 is possible by observing that the recycle of Q becomes infinitely large as $m \rightarrow m_1$. To verify this, it is sufficient to note that the reactor conversion of A approaches zero as $m \rightarrow m_1$. Since finite amounts of A and B are fed to the reactor, this can be only due to infinite recycle of Q. As the recycle of Q becomes infinitely large and reactor conversion approaches zero, concentrations and temperature are constant along the reactor. Hence, the reactor behaves as a CSTR operated at the feed temperature. For this reason, the dependence of m_1 on system parameters can be predicted by replacing the plug-flow reactor model by a CSTR model and solving it jointly with the condition $x_A = 0$. This gives the following inequality guaranteeing the existence of feasible steady states:

$$\frac{m}{p} \leq K_{2,1} \tag{18}$$

where the equality holds at $m = m_1$.

On the basis of (18), a limit reactor-inlet flow rate of B, $p_1 = m/K_{2,1}$, can be equivalently determined. Once m is given, feasible steady states are guaranteed to exist for $p > p_1$.

Inequality 18 guarantees that feasible steady states can be found when the ratio m/p, between the reactor-inlet flow rates of the endothermic reactant A and of the exothermic reactant B, is lower than the ratio $K_{2,1} = k_2/k_1$, between the kinetic constants of the exothermic and of the endothermic reactions. To explain this result, we remark that steady state operation of the reactor−separation−recycle system requires that the amount of Q produced by the endothermic reaction is completely converted by the exothermic reaction. When the reactor behaves as a CSTR, this is equivalent to require the matching of the reaction rates evaluated at the reactor outlet conditions:

$$k_1 w_A = k_2 w_B w_Q \tag{19}$$

where w_A, w_B, and w_Q are the reactor outlet molar fractions of the species A, B, and Q, respectively. On the other hand, in the limit $m \rightarrow m_1$, reactor conversion approaches zero and a finite amount of heat is transferred to the infinite flow through the reactor, resulting in identical conditions of the outlet and inlet streams. Therefore, eq 19 can be recast in the following form:

$$k_1 m = k_2 p w_Q \tag{20}$$

Inequality 18 follows from (20) by noting that $w_Q \leq 1$.

Inequality 18 defines an operating region where feasible steady states exist. In the following, we derive conditions under which a unique steady state is found.

In Figure 5, four saddle-node bifurcation points S_1, S_2, S_3 and S_4 delimitate m ranges where three steady states coexist. Projections of the saddle-node bifurcation locus on the $m-p$ plane are displayed in Figure 6 at four decreasing $K_{2,1}$ values.

In each plot, it is also shown the evolution of the limit point $m_1(p)$. According to eq 18, this is a straight line with slope equal to the kinetic ratio $K_{2,1}$. Two distinct branches are invariably found describing the evolution of the saddle-node bifurcation points (S_1, S_2) and (S_3, S_4).

When $K_{2,1} > 1$ (Figure 6a and b), the branches of saddle-node bifurcation points mainly extend in the region $m > p$ and a unique steady state is detected for the largest part of the region $p > m$. To qualitatively explain this behavior, we observe that, at similar activation energies or high heat transfer capacity, $p > m$ and $K_{2,1} > 1$ imply that the exothermic reaction is faster than the endothermic one along the reactor. Under these conditions, the amount of Q leaving the reactor and being recycled is negligible. Hence, the system behaves as a reactor−separation−recycle system where, at the reactor-inlet, the flow rates of all reactants are fixed.

For $K_{2,1} < 1$ (Figure 6c and d), the saddle-node bifurcation branch corresponding to the points S_1 and S_2 invariably extends in the region $m > p$ and a boundary-limit point (p_2, m_2) is detected, through which the point S_3 vanishes. This can be seen in Figure 7, showing the evolution of the steady state solution diagram, with m as bifurcation parameter, as p varies, at $K_{2,1} = 0.4$.

As p is reduced, the reactor conversion attained at the saddle-node bifurcation point S_3 becomes smaller and smaller and approaches zero as $p \rightarrow p_2$. We recall that, in the limit $x_A \rightarrow 0$, the recycle of Q becomes infinitely large and the plug-flow reactor behaves as a CSTR. Hence, the dependence of the limit point (p_2, m_2) on model parameters can be predicted by solving the CSTR model jointly with the defining condition of a saddle-node bifurcation point and the condition $x_A = 0$. Obviously, condition 18 holds, giving $m_2 = m_1(p_2) = K_{2,1}p_2$. Furthermore, the following relationships governing the dependence of (m_2, p_2) on system parameters are obtained:

$$p_2 = \frac{Da(1 - K_{2,1})}{2(1 + K_{2,1})} \quad m_2 = K_{2,1}\frac{Da(1 - K_{2,1})}{2(1 + K_{2,1})} \tag{21}$$

It is apparent, from Figure 6, that steady state multiplicity can be avoided, when $K_{2,1} < 1$, by selecting m and p values fulfilling the following conditions:

$$p \leq p_2; \quad m \leq pK_{2,1} \tag{22}$$

The safe region described by eq 22 results from the intersection of the curve spanned by the limit point (p_2, m_2) as $K_{2,1}$ is varied (eqs 21) and the straight line $m = pK_{2,1}$, as shown in Figure 8.

It can be observed that the safe region becomes smaller and smaller as Da and $K_{2,1}$ decrease.

Control Strategy C_2. The system to be solved to determine the steady state solution regimes of the reactor−separation−recycle system controlled by strategy C_2 is described by eqs 1–3 and the following additional equations:

$$f_{A,1} - m = 0 \tag{23}$$

$$f_{B,1} + f_{Q,1} - p = 0 \tag{24}$$

The parameters m and p define the reactor-inlet flow rate of A and the sum of the reactor-inlet flow rates of B and Q, respectively.

Steady state solution regimes are described in Figure 9a as m varies, at $p = 4$. The reactor conversion of A is employed as variable representative of the state of the system. Three saddle-node bifurcation points S_1, S_2, and S_3 are predicted. At low m values, two coexisting steady states are detected. As m is increased, four steady states coexist in the range delimitated by the points S_1 and S_2. At larger m values, two steady states vanish through the point S_2 and two coexisting steady states are detected between the points S_2 and S_3. Feasible steady states vanish through the point S_3 and are not detected as m is further increased.

Saddle-node bifurcation points S_1, S_2, and S_3 define operability limits delimitating a region where four steady states coexist and a region where feasible steady states are not detected. Therefore, they need to be predicted to select m and p values guaranteeing plant operability.

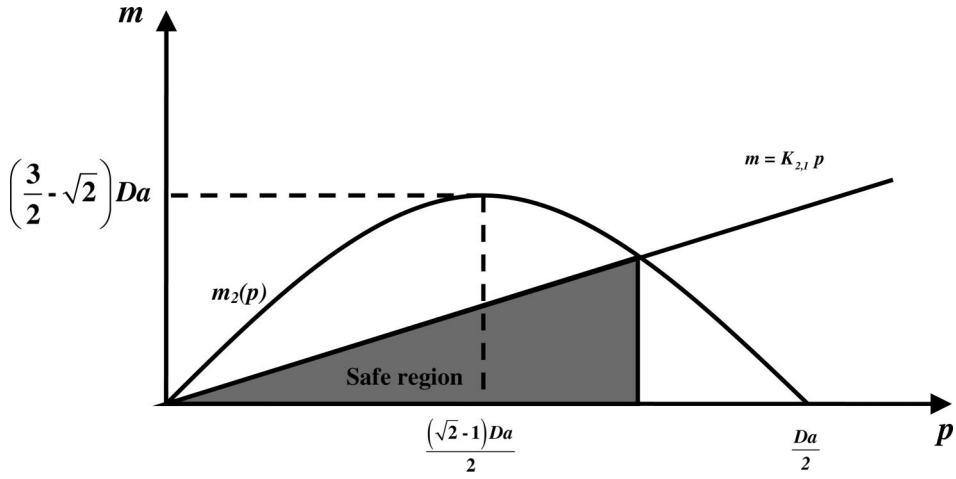

Figure 8. Construction of the safe region of the set-point variables space at kinetic constant ratio values $K_{2,1} < 1$.

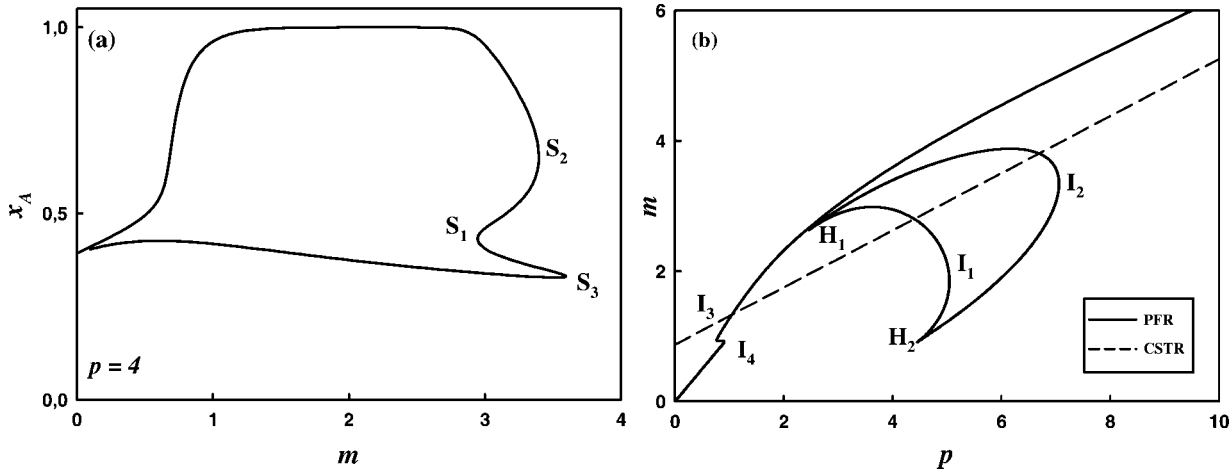

Figure 9. Bifurcation structure of the PFR−separation−recycle system controlled by strategy C_2. (a) Steady state solution diagram, with m as a bifurcation parameter, at $p = 4$. (b) Projection of the saddle node bifurcation points on the $m-p$ plane ($Da = 2$, $K_{2,1} = 2.5$, $B = 0.3$, $\beta = 0.01$, $\gamma = 12.5$, $G_{2,1} = 2.5$, $H_{2,1} = 4.5$, $\theta_c = 0$).

The projection of the locus of saddle-node bifurcation points on the $m-p$ plane is shown in Figure 9b. Two separate bifurcation branches are detected as m and p vary: a closed branch delimitated by the cusp points H_1 and H_2 and the isola points I_1, I_2 and a branch extending over the unbounded range $p \in [0, +\infty)$ along which the isola points I_3, I_4 are detected. The latter branch describes the evolution of the saddle-node bifurcation point S_3 (Figure 9a) and divides the $m-p$ plane into two regions: the upper region, where feasible steady states are not detected, and the lower region, where feasible steady states exist.

It is apparent, from Figure 9b, that the evolution of the saddle-node bifurcation point S_3, follows, at large p, a straight line. An approximation for this can be obtained by observing that the flow rate through the reactor becomes infinitely large in the limit $p \rightarrow +\infty$. Under these conditions, the bifurcation structure of the plant can be predicted by replacing the steady state plug-flow model with the steady state model of a CSTR. This leads to the following inequality guaranteeing, in the limit $p \rightarrow +\infty$, the existence of feasible steady states:

$$m \leq \frac{(\sqrt{(1+K_{2,1})}-1)(Da+p)}{2} \qquad (25)$$

where the equality holds at the saddle-node bifurcation point S_3. According to (25), the relationship between the m and p values corresponding to the point S_3 is, in the limit $p \rightarrow +\infty$, linear and is only affected by the Damköhler number Da and the kinetic constant ratio $K_{2,1}$. The evolution of the saddle-node bifurcation point S_3 predicted by (25) is shown in Figure 9b. Obviously, inequality 25 provides a misleading description of the feasibility boundary at low p values. However, a conservative approximation holds at slightly larger p values, allowing inequality 25 to be usefully employed to detect feasible m and p values in wide p ranges. For example, initial guesses for m and p could be found based on (25).

It results, from inequality 25, that increasing $K_{2,1}$ enlarges the feasible operating region. This can be qualitatively explained by remarking that steady state operation of the reactor−separation−recycle system requires that the amount of Q produced by the endothermic reaction is completely converted by the exothermic reaction. In general, this is possible if the exothermic reaction is sufficiently faster than the endothermic reaction. On the other hand, at infinite recycle rates, the reactor behaves as a CSTR operated at the feed temperature. Hence, guaranteeing high rate of the exothermic reaction is equivalent to require that the ratio $K_{2,1}$, between the kinetic constants of the exothermic and endothermic reactions, evaluated at the reactor-inlet temperature, is sufficiently high.

On the contrary, increasing Da moves the feasibility boundary in the positive direction of the p axis. Hence, given p and $K_{2,1}$,

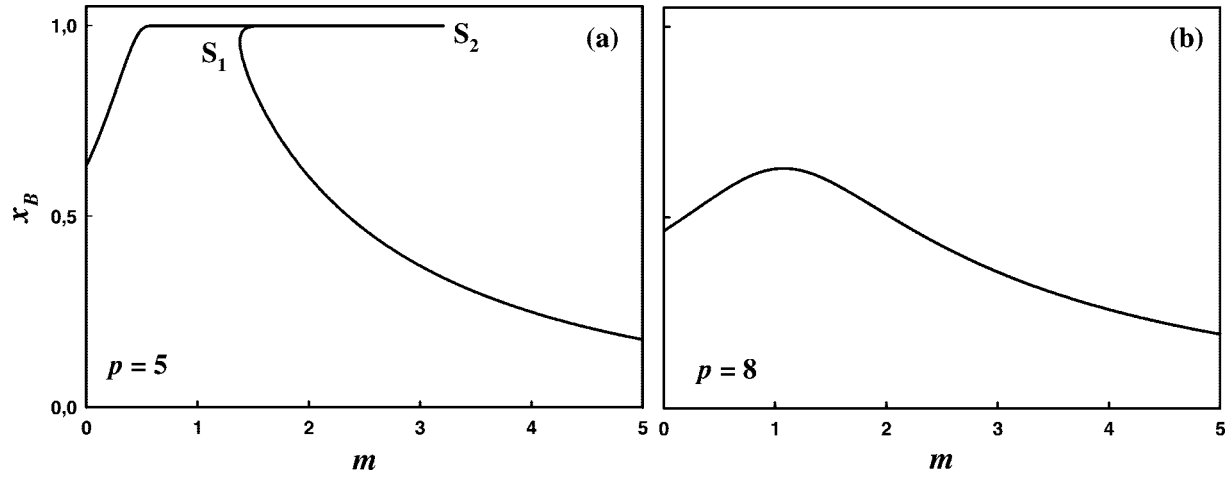

Figure 10. Steady state solution diagrams of the PFR−separation−recycle system controlled by strategy C_3, with m as bifurcation parameter, at $p = 4$ (a) and $p = 8$ (b) ($Da = 2$, $K_{2,1} = 2.5$, $B = 0.3$, $\beta = 0.01$, $\gamma = 12.5$, $G_{2,1} = 2.5$, $H_{2,1} = 4.5$, $\theta_c = 0$).

the saddle-node bifurcation point S_3 is expected to occur at lower m values as Da is increased.

Control Strategy C_3. Characterizing the steady state behavior of the reactor−separation−recycle system controlled by strategy C_3 requires to solve equations 1–3 jointly with the following additional equations:

$$f_{B,1} - m = 0 \tag{26}$$

$$f_{A,1} + f_{Q,1} - p = 0 \tag{27}$$

where m and p define the reactor-inlet flow rate of B and the sum of the reactor-inlet flow rate of A and Q, respectively.

Steady state solution regimes are described in Figure 10 as m varies, at two different p values. The reactor conversion of B is picked as a variable representative of the state of the system. At $p = 5$, two saddle-node bifurcation point S_1 and S_2 delimitate a range where three steady state solution regimes coexist (Figure 10a). Two of these regimes present close conversion values resulting barely distinguishable in Figure 10a. As m is increased, a unique steady state is detected at which reactor conversion decreases approaching zero in the limit $m \to +\infty$. At larger p values, saddle-node bifurcation points are not predicted and a unique steady state is invariably detected as m varies (Figure 10b).

At $p = 5$, three coexisting steady states are detected as m ranges between the points S_1 and S_2. Under these conditions, the basin of attraction of the desired regime could be very narrow. For this reason, it is important to predict the evolution of the points S_1 and S_2 as system parameters vary.

The projection of the saddle-node bifurcation locus on the $m-p$ plane is shown in Figure 11. A closed branch is observed dividing the parameter space into two regions: the external region, where a unique steady state exists, and the internal region, where steady state multiplicity is experienced. As m and p vary, six isola points I_1-I_6 and two cusp points H_1 and H_2 are detected.

It is important to observe that no feasibility boundaries arise. Hence, feasible steady states are invariably detected as m and p vary. Furthermore, steady state multiplicity vanishes at large p and/or m values.

4.2. Control Strategies Exploiting the Self-Regulation Property. Control Strategy C_4. Let us consider the PFR−separation−recycle system controlled by strategy C_4. The system to be solved in order to determine the steady state solution

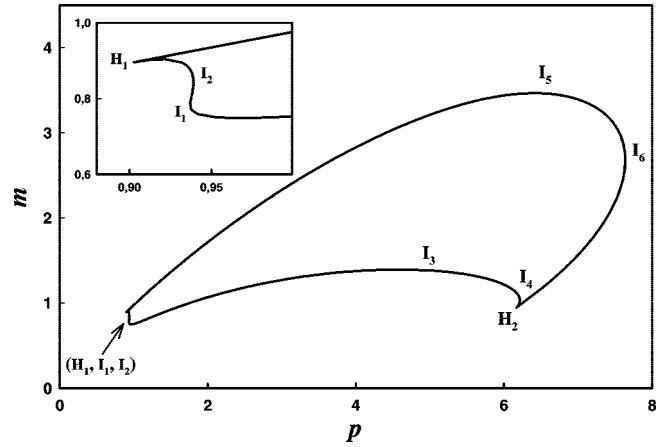

Figure 11. Projection of the saddle node bifurcation points of the PFR−separation−recycle system controlled by strategy C_3 on the $m-p$ plane ($Da = 2$, $K_{2,1} = 2.5$, $B = 0.3$, $\beta = 0.01$, $\gamma = 12.5$, $G_{2,1} = 2.5$, $H_{2,1} = 4.5$, $\theta_c = 0$).

regimes is described by equations 1–3 and the following additional equations:

$$f_{A,0} - m = 0 \tag{28}$$

$$f_{B,0} + f_{A,3} + f_{B,3} - p = 0 \tag{29}$$

The parameter m defines the fresh feed flow rate of A and the parameter p defines the sum of the reactor-inlet flow rate of B and of the recycle flow rate of A. Since reaction stoichiometry imposes $f_{A,0} = f_{B,0}$, eq 29 can be recast in the following form:

$$f_{A,3} + f_{B,3} = p - m \tag{30}$$

Hence, in order to guarantee feasibility (positive flow rates) of steady state solution regimes, parameters m and p must fulfill the following:

$$p > m \tag{31}$$

It should be observed that, according to eq 30, $p - m$ gives the flow rate of the recycle stream ((A, B) recycle, Figure 3b), used in implementing the control strategy C_4 (Figure 4 C_4). It is remarkable that this observation holds for all the control strategies exploiting the self-regulation property (C_4-C_8). For example, for the control strategy C_5, $p - m$ gives the flow rate of the recycle (A, Q) appearing in the corresponding control

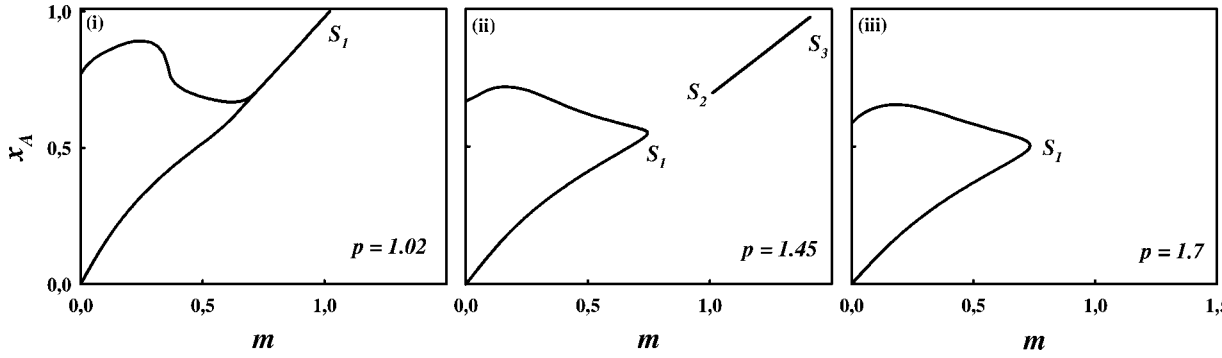

Figure 12. Qualitatively different steady state solution diagrams of the PFR−separation−recycle system controlled by strategy C_4, with m as a bifurcation parameter, observed as p varies ($Da = 1.5$, $K_{2,1} = 1.5$, $B = 0.25$, $\beta = 0.01$, $\gamma = 12.5$, $G_{2,1} = 2.5$, $H_{2,1} = 5$, $\theta_c = 0$).

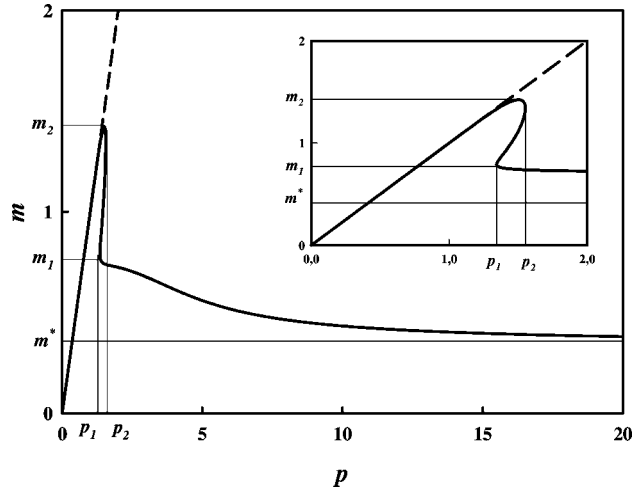

Figure 13. Projections of the saddle node bifurcation points of the PFR−separation−recycle system controlled by strategy C_4 on the $m-p$ plane ($Da = 1.5$, $K_{2,1} = 1.5$, $B = 0.25$, $\beta = 0.01$, $\gamma = 12.5$, $G_{2,1} = 2.5$, $H_{2,1} = 5$, $\theta_c = 0$).

structure (Figure 4 C_5). For this reason, inequality 31 invariably applies to control strategies C_4-C_8.

Steady states of the reactor−separation−recycle system are described in Figure 12 as m is varied, at three increasing p values.

The reactor conversion of A is selected as variable representative of the state of the system. At $p = 1.02$ (Figure 12i), two steady states coexist at low m values. As m is increased, a saddle-node bifurcation point S_1 is detected leading to the disappearance of feasible steady states.

As p is increased (Figure 12ii), an isolated steady state solution branch delimitated by the saddle-node bifurcation points S_2 and S_3 arises. Two barely distinguishable steady states coexist on this branch. At larger p values (Figure 12iii), the solution diagram is qualitatively identical to the solution diagram displayed in Figure 12i.

Saddle-node bifurcation points displayed in Figure 12 define operability limits of the reactor−separation−recycle system delimitating m ranges where feasible steady states are not detected. Hence, they must be predicted to select m and p values guaranteeing feasible operation.

Figure 13 shows m and p values at which saddle-node bifurcation points are detected.

The locus of saddle-node bifurcation points divides the $m-p$ plane into a region where feasible steady states are not detected and a region where feasible steady states exist.

As p varies, three qualitatively different steady state solution diagrams with m as bifurcation parameter are observed. They are described in Figure 12i−iii and correspond to p ranges $p \in [0, p_1]$, $p \in [p_1, p_2]$, $p \in [p_2, +\infty)$, respectively. Two isola points are detected at p_1 and p_2 leading to the appearance (Figure 12ii) and to the disappearance (Figure 12iii) of an isolated steady state solution branch.

As m varies, two qualitatively different steady state solution diagrams with p as bifurcation parameter are observed. They are displayed in Figure 14i and ii and correspond to the m ranges $m \in [m^*, m_2]$ and $m \in [0, m^*]$, respectively.

At m values larger than m_2, feasible steady states are not detected as p is varied. As m is decreased, an isola point leads, at m_2, to the appearance of an isolated steady state solution branch. At m values belonging to the range $m \in [m^*, m_2]$, two steady states coexist as p varies in the range delimitated by the saddle-node bifurcation points S_1 and S_2 (Figure 14i).

Figure 13 shows that, as m is decreased over the range $m \in [m_1, m_2]$, the saddle-node bifurcation point S_1 approaches the limit (31) and the saddle-node bifurcation point S_2 shifts at lower p values. However, as the value m_1 is crossed and m is decreased over the range $m \in [m_1, m^*]$, the p value corresponding to the point S_2 rapidly rises and goes to infinity as $m \rightarrow m^*$. At m values lower than m^* (Figure 14ii), feasible steady states are invariably detected as p varies over the unbounded range $p \in [m, +\infty)$. Therefore, the m^* value provides a valuable indication on how to select m to guarantee feasible operation.

From this perspective, it should be remarked that analytical prediction of m^* is possible. To this end, we observe that, in the limit $m \rightarrow m^*$, the flow rate through the reactor, corresponding to the saddle-node bifurcation point S_2, becomes infinitely large. Hence, we can use the CSTR approximation previously explained. This gives the following inequality guaranteeing existence of feasible steady states:

$$K_{2,1} \geq \frac{4mDa}{(Da - m)^2}, \quad m \in [0, Da] \tag{32}$$

where the equality holds at $m = m^*$. Application of (32) outside the range $m \in [0, Da]$ is not allowed leading to unfeasible saddle-node bifurcation points. According to (32), m^* only depends on Da and $K_{2,1}$.

Inequality 32 can be qualitatively explained by recalling that, in the CSTR asymptote, the amount of Q produced by the exothermic reaction can be completely converted by endothermic reaction only if the kinetics ratio $K_{2,1}$ is sufficiently high.

Figure 15 describes the evolution of m^* as $K_{2,1}$ is varied, at four Da values. Each curve divides the $m-K_{2,1}$ plane into two regions: the lower one, where feasible steady states are detected as p varies, and the upper one, where feasible operation cannot be guaranteed.

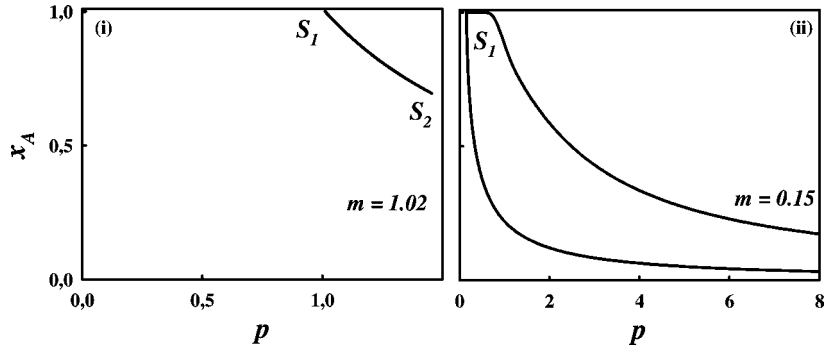

Figure 14. Qualitatively different steady state solution diagrams of the PFR−separation−recycle system controlled by strategy C_4, with p as a bifurcation parameter, observed as m varies ($Da = 1.5$, $K_{2,1} = 1.5$, $B = 0.25$, $\beta = 0.01$, $\gamma = 12.5$, $G_{2,1} = 2.5$, $H_{2,1} = 5$, $\theta_c = 0$).

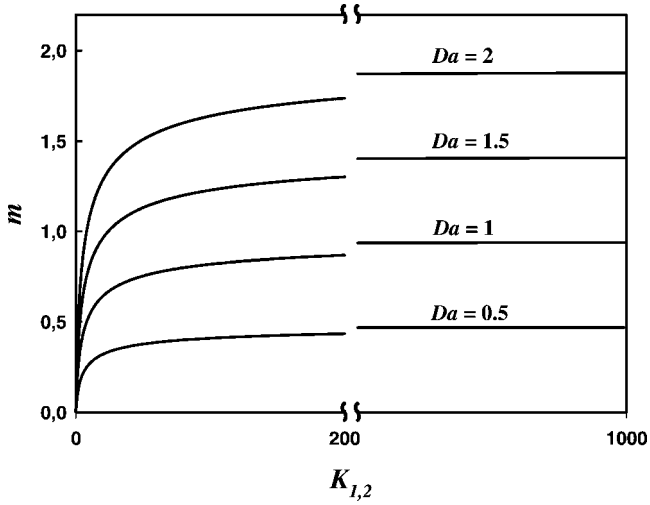

Figure 15. Evolution of the limit value m^* as the kinetic ratio $K_{1,2}$ is varied at different Da values ($B = 0.25$, $\beta = 0.01$, $\gamma = 12.5$, $G_{2,1} = 2.5$, $H_{2,1} = 5$, $\theta_c = 0$).

As $K_{2,1}$ varies, m^* invariably increases and approaches Da as $K_{2,1} \rightarrow +\infty$. Hence, at $m \geq Da$, independently of the kinetic constant ratio $K_{2,1}$, feasible steady states are detected over bounded p ranges.

Control Strategies C_5−C_8. Figure 16 displays projections on the m−p plane of the loci of the saddle-node bifurcation points of the PFR−separation−recycle system controlled by strategies C_5−C_8.

It is apparent, from Figure 16, that these control strategies produce bifurcation structures more complex than control strategy C_4 (Figure 14). Qualitatively identical bifurcation structures are observed for control strategies C_5 and C_7 and for control strategies C_6 and C_8. When the strategy C_5 and C_7 are implemented (Figure 16a and c), two isola points I_1 and I_2 and two cusp points H_1 and H_2 are detected as m and p are varied leading to several qualitatively different steady state solution diagrams. When the control strategy C_6 and C_8 are implemented (Figures 16b and d), two separated saddle-node bifurcation branches arise where five isola points (I_1, I_2, I_3, I_4, I_5) and two cusp points (H_1, H_2) are detected as m and p are varied.

We wish to emphasize some analogies between control strategies C_4−C_8 useful in selecting m and p values guaranteeing feasible operation. Projections of the saddle-node bifurcation points displayed in Figure 16 define feasibility boundaries of the reactor−separation−recycle system. They divide the m−p plane into a region where feasible steady states are not detected and a region where feasible steady states exist. Furthermore, as observed for control strategy C_4, a limit m value is detected, for control strategies C_5−C_8, under which steady states arise as p varies in the unbounded range $p \in [m, +\infty)$. This limit value can be predicted by replacing the plug-flow reactor model with a CSTR model and solving the defining conditions of a saddle-node bifurcation point in the limit $p \rightarrow +\infty$, invariably leading to inequality 32.

5. Conclusions

The steady state behavior of PFR−separation−recycle systems, where the first order endothermic reaction A → R + Q and the second order exothermic reaction B + Q → P simultaneously take place, was thoroughly investigated. Flowsheets of the reactor−separation−recycle system which are possible, as the physical properties of the species involved vary, were classified, and control strategies were suggested. In this contribution, results concerning the behavior of the system were shown for eight control strategies. In particular, three control strategies based on feedback control of reactants inventory (C_1, C_2, C_3) and five control strategies exploiting plant self-regulation (C_4, C_5, C_6, C_7, C_8) were considered.

Bifurcation analysis was performed as the set-points of the flow control loops are varied providing guidelines for safe plant operation.

For control strategy C_1, limit values for the reactor-inlet flow rates of A and B were analytically predicted, approaching which steady state conversion goes to zero (eq 18). When the reactor-inlet flow rate of A (respectively B) is lower (respectively greater) than the corresponding limit value, feasible steady state solution regimes can be always found. Guidelines to avoid the occurrence of state multiplicity during plant operation were also provided. In particular, at kinetic ratios $K_{2,1} > 1$, a unique steady state exist when the reactor-inlet flow rate of B is greater than the reactor-inlet flow rate of A. At $K_{2,1} < 1$, a boundary limit variety was found delimitating a region of the set-point variables space where a unique steady state is detected (eqs 21 and 22).

For control strategy C_2, a saddle-node bifurcation point was predicted crossing which feasible steady states vanish. An analytical description for the evolution of this point in the space of the set-point variables was obtained providing a conservative approximation of the feasibility boundary (eq 25).

For control strategy C_3, feasible steady states were invariably detected as system parameters vary and a closed saddle-node bifurcation branch was computed dividing the space of the set-point variables into a region where steady state multiplicity occurs and a region where a unique steady state is detected.

For control strategies exploiting the self-regulation property (C_4, C_5, C_6, C_7, C_8), saddle-node bifurcation points divide the space of the set-point variables into an unfeasible region, where feasible steady states are not detected, and a feasible region, where feasible steady states exist. Furthermore, a region of the

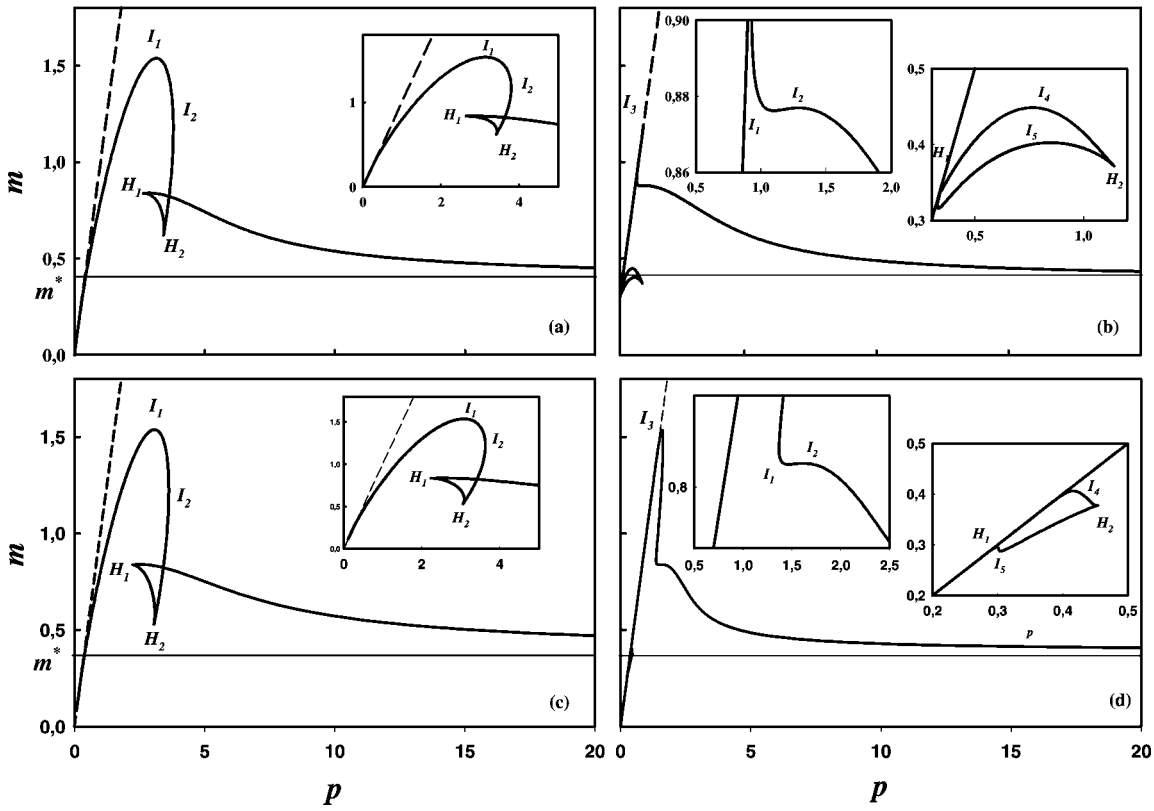

Figure 16. Projections of the saddle node bifurcation points of the PFR−separation−recycle system controlled by strategy C_5 (a), C_6 (b), C_7 (c), and C_8 (d) on the $m-p$ plane ($Da = 2$, $K_{2,1} = 1.2$, $B = 0.3$, $\beta = 0.01$, $\gamma = 12.5$, $G_{2,1} = 2.5$, $H_{2,1} = 4.5$, $\theta_c = 0$).

set-point variables space was computed where the reactor−separation−recycle system exhibits feasible steady states (eq 32).

It is remarkable that no control strategy is found ruling out the occurrence of state multiplicity. This must be mainly attributed to the class of chemical processes considered in this paper. It involves three reactants, whereas plantwide control allows fixing only two degrees of freedom. For this reason, the steady state behavior of the plant is invariably affected by material recycle effects, making nonlinear analysis an indispensable step toward the identification of safe operating regions.

From this perspective, results presented in this paper should draw the attention of industrial practitioners and designers to the possibility of serious risks for plant safety. The choice of the optimal plant operating point is frequently performed on the basis of economic arguments and production requirements. In practice, a constrained optimization problem must be solved. However, when a thorough description of the bifurcation/feasibility boundaries of the system is not taken into account, optimizing an economic index may produce an operating point, in practice, unfeasible. For example, the resulting point may be close to a saddle node bifurcation boundary. In this case, slight disturbances, always present in industrial practice, or unavoidable model uncertainties could lead to an undesired transition regime, such as, for example, plant shutdown.

In order to prevent the occurrence of such undesired phenomena, feasibility constraints guaranteeing robustness of the selected operating point must be necessarily added to the optimization problem. To this regard, a new approach has been presented over the past few years which enable the optimization-based design of continuous processes in presence of model and parametric uncertainty.[24] Nevertheless, the efficient implementation of these methodologies is prevented by the lack of an explicit characterization of the process feasibility boundaries. These are, in general, described in implicit form and are computed by solving large nonlinear systems of equations. However, analytical feasibility conditions provided throughout the paper may be used to replace this description guaranteeing the possibility to efficiently detect a robust plant operating point. This could be used, for example, as initial guess for a more rigorous process optimization.

In line with this approach, the results presented in this paper are, in general, expected to provide valuable guidelines for future studies aimed to improve the understanding of the nonlinear behavior of plantwide systems simultaneously coupling exothermic and endothermic reactions. In this direction, we consider the analysis of specific examples and the implementation of detailed plant models an indispensable step toward a broader characterization of system nonlinearities. Nevertheless, we wish to stress the importance that a qualitative description of the bifurcation structure of system can have while coping with detailed process models. The analysis provided throughout the paper could be, for example, used in order to reduce lengthy and tedious design iterations which sometimes result from the implementation of detailed models in plant simulation software. In these applications, the use of reliable high dimensional plant models prevents the possibility to efficiently perform a detailed bifurcation analysis. Rather, the approach is fixing all the plant parameters and using efficient nonlinear solvers to detect a single stationary point. However, this point may be close to a bifurcation boundary. Hence, when the plant is operated at this point, slight disturbances could give rise to undesired transition regimes. This could be recognized only by performing dynamic simulations of the plant model. It should be clear that the unsuccessful selection of plant stationary points may eventually lead to lengthy and tedious iterations. In this framework, our analysis reduces the risk of design failures by providing, within a very general modeling setting, an explicit characterization of

the plant feasibility boundaries. Furthermore, we consider a qualitative understanding of process nonlinearities central for providing effective physical interpretations of the results of more specific studies.

It is worth to conclude remarking that the results presented in this paper do not exhaust the analysis of the bifurcation structure of the reactor−separation−recycle system. Indeed, no information is provided concerning the stability characteristics of stationary solution branches and the possible detection of dynamic bifurcations. Nonlinear dynamics of the reactor−separation−recycle system lives from the interaction between dynamics of the locally controlled separation and reactor units. Even when the dynamics of the stand alone controlled units do not exhibit undesired features, reactor−separation couplings have been frequently proved to be responsible for undesired dynamic transition regimes. Nevertheless, analyzing the dynamic behavior of the reactor−separation−recycle system would require defining a dynamic model for the controlled separation unit. The formulation of this model would be invariably affected by the selection and design of the separation controller structure. This would dramatically limit the generality of a dynamic analysis. In this perspective, further developments of this work, should rather investigate the possibility to define, for a given class of reactors, what characteristics the local dynamics of the separation units should exhibit in order to reduce the risk of undesired dynamic bifurcations. According to this approach, the design of the separation controller structure should not be driven by traditional controller techniques, but rather aimed to tailor a desired separation dynamics.

Nomenclature

B = adiabatic temperature rise, dimensionless, $\Delta H_1/[C_p T_1]$
C_p = specific heat (J/(mol K))
D = reactor diameter (m)
Da = Damköhler number, dimensionless, $k_1(T_1)[V/F_0]$
E_K = activation energy (J/mol)
f_k = flow rate, dimensionless, F_k/F_0
F = flow rate (mol/s)
$G_{2,1}$ = ratio of activation energies, dimensionless, E_2/E_1
ΔH_K = heat of reaction (J/mol)
$H_{2,1}$ = ratio of heat of reactions, dimensionless, $-\Delta H_2/\Delta H_1$
k = pre-exponential factor (mol/(m^3 s))
$K_{2,1}$ = ratio of pre-exponential factors, dimensionless, $k_2(T_1)/k_1(T_1)$
L = reactor length (m)
R = gas constant (J/(mol K))
T = temperature (K)
U = heat-transfer coefficient (W/(m^2 K))
V = reactor volume (m^3)
w_X = molar fraction of X
x_A = conversion of A
x_B = conversion of B
z = axial coordinate (m)

Greek Symbols

β = heat-transfer capacity, dimensionless, $4U/[Dk_1(T_1)C_p]$
γ = activation energy, dimensionless, E/RT_1
θ = temperature, dimensionless, $[T - T_1]/T_1$
ξ = axial coordinate, dimensionless, z/L

Subscripts

X = reactant A, B, or Q
X0 = X in fresh feed
X1 = X in reactor inlet
X2 = X in reactor outlet
X3 = X in recycle
1 = endothermic reaction, A → R + Q
2 = exothermic reaction, B + Q → P
0 = reference
c = coolant

Literature Cited

(1) Towler, G.; Lynn, S. Novel applications of reaction coupling: use of carbon dioxide to shift the equilibrium of dehydrogenation reactions. *Chem. Eng. Sci.* **1994**, *49*, 2585.

(2) Grasselli, R. K.; Stern, D. L.; Tsikoyiannis, J. G. Catalytic dehydrogenation of light paraffins (DH) combined with selective hydrogen combustion (SHC) •I•DH → SHC → DH catalysts in series (co-fed process mode). *Appl. Catal. A: Gen.* **1999**, *189*, 1.

(3) Grasselli, R. K.; Stern, D. L.; Tsikoyiannis, J. G. Catalytic dehydrogenation of light paraffins (DH) combined with selective hydrogen combustion (SHC) •I•DH → SHC → DH catalysts physically mixed (redox process mode). *Appl. Catal. A: Gen.* **1999**, *189*, 9.

(4) Henning, D. A.; Schmidt, L. D. Oxidative dehydrogenation of ethane at short contact times: species and temperature profiles within and after the catalyst. *Chem. Eng. Sci.* **2002**, *57*, 2615.

(5) Chaudhary, V. R.; Rane, V. H.; Rajput, A. M. High temperature catalytic oxidative conversion of propane to propylene and ethylene involving coupling of exothermic and endothermic reactions. *Ind. Eng. Chem. Res.* **2000**, *39*, 904.

(6) Hickman, K. L.; Schmidt, L. D. Production of synthesis gas by direct oxidation of methane. *Science* **1993**, *259*, 343.

(7) De Groote, A. M.; Froment, G. F. Simulation of the catalytic partial oxidation of methane to synthesis gas. *Appl. Catal. A: Gen.* **1996**, *138*, 245.

(8) Hohn, K. L.; Schmidt, L. D. Partial oxidation of methane to syngas at high space velocities over Rh-coated spheres. *Appl. Catal. A: Gen.* **2001**, *211*, 53.

(9) Qin, Z.; Liu, J.; Sun, A.; Wang, J. Reaction coupling in the new processes for producing styrene from ethylbenzene. *Ind. Eng. Chem. Res.* **2003**, *42*, 1329.

(10) Pushpavanam, S.; Kienle, A. Nonlinear behavior of an ideal reactor separator network with mass recycle. *Chem. Eng. Sci.* **2001**, *56*, 2837.

(11) Kiss, A. A.; Bildea, C. S.; Dimian, A. C.; Iedema, P. D. State multiplicity in CSTR-separator-recycle polymerization systems. *Chem. Eng. Sci.* **2002**, *57*, 535.

(12) Kiss, A. A.; Bildea, C. S.; Dimian, A. C.; Iedema, P. D. State multiplicity in PFR-separator-recycle polymerization systems. *Chem. Eng. Sci.* **2003**, *58*, 2973.

(13) Bildea, C. S.; Dimian, A. C. Fixing flow rates in recycle systems: Luyben's rule revisited. *Ind. Eng. Chem. Res.* **2003**, *42*, 4578.

(14) Luyben M. L., Luyben W. L. *Essentials of Process Control*; McGraw-Hill: New York, 1997.

(15) Antelo, L. T.; Otero-Muras, I.; Banga, F. R.; Alonso, A. A. A systematic approach to plant-wide control based on thermodynamics. *Comput. Chem. Eng.* **2007**, *31*, 677.

(16) Jillson, K. R.; Ydstie, B. E. Process networks with decentralized inventory and flow control. *J. Process Control* **2007**, *17*, 399.

(17) Baldea, M.; Daoutidis, P.; Kumar, M. Dynamics and Control of Integrated Networks with Purge Streams. *AIChE J.* **2006**, *52*, 1460.

(18) Baldea, M.; Daoutidis, P. Control of integrated process networks—A multi-time scale perspective. *Comput. Chem. Eng.* **2007**, *31*, 426.

(19) Luyben, M. L.; Tyreus, B. D.; Luyben, W. L. Plantwide control design procedure. *AIChE J.* **1997**, *43*, 3161.

(20) Gilles, E. D.; Lauschke, G.; Kienle, A.; Storz, M. Some aspects of integrated process operation. *A. Rev. Control.* **1996**, *20*, 9.

(21) Downs J. Distillation Control in a Plantwide Control Environment. In *Practical Distillation Control*; Luyben, W., Ed.; van Nostrand Rheinhold: New York, 1992.

(22) Golubitsky M., Schaffer D. *Singularity and groups in bifurcation theory*; Springer: New York, 1985.

(23) Subramanian, S.; Balakotaiah, V. Classification of the steady state and dynamic behavior of distributed reactor models. *Chem. Eng. Sci.* **1996**, *51*, 401.

(24) Monnigmann, M.; Marquardt, W. Steady-state process optimization with guaranteed robust stability and feasibility. *AIChE J.* **2003**, *49*, 3110.

Received for review October 11, 2007
Revised manuscript received May 30, 2008
Accepted June 9, 2008

IE071367G